Nano Research 14.2 (2020): 458-465

DOI: https://doi.org/10.1007/s12274-020-2779-8

Rational Design of Heterogeneous Catalysts with Programmable Topologies by Reticulation of Organocatalysts into Metal-Organic Frameworks: the Case of Squaramide

Anna Broto-Ribas[†], *Claudia Vignatti,*[†] *Javier Luis-Barrera,*[‡] *Alicia Jimenez-Almarza,*[§] *Zahra Dolatkhah*[‡], *Inhar Imaz,*[†,*] *Rubén Mas-Ballesté,*[§,#*] *José Alemán*[‡,#*] *and Daniel Maspoch*[†,⊥*]

† Catalan Institute of Nanoscience and Nanotechnology (ICN2), CSIC and The Barcelona Institute of Science and Technology, Barcelona, Spain

‡ Organic Chemistry Department, Módulo 1, Universidad Autónoma de Madrid, Madrid, Spain

§ Inorganic Chemistry Department, Módulo 7, Universidad Autónoma de Madrid, Madrid, Spain

Institute for Advanced Research in Chemical Sciences (IAdChem), Campus Universidad Autónoma de Madrid, Madrid, Spain

⊥ Institució Catalana de Recerca i Estudis Avançats (ICREA), Barcelona, Spain

KEYWORDS: Reticular Chemistry, Metal-Organic Frameworks, H-bond catalysis, Squaramide, Friedel-Crafts, Epoxide ring-opening

ABSTRACT:

A well-established strategy to synthesize heterogeneous, metal-organic framework (MOF) catalysts that exhibit nanoconfinement effects, and specific pores with highly-localized catalytic sites, is to use organic linkers containing organocatalytic centers. Here, we report that by combining this linker approach with reticular chemistry, and exploiting 3D MOF-structural data from the Cambridge Structural Database, we have designed four new, heterogeneous MOF-based catalysts for standard organic transformations. These programmable MOFs are isoreticular versions of **pcu-IRMOF-16**, **fcu-UiO-68** and **pillared-pcu-SNU-8X**, the three most common topologies of MOFs built from the organic linker *p*,*p*'-terphenyldicarboxylic acid (**tpdc**). To synthesize the four squaramide-based MOFs, we designed and synthesized a linker, 3,4-dioxocyclobut-1-ene-1,2-diyl)bis(azanedyil)-*p*-dibenzoic acid) (**Sq_tpdc**), which is identical in directionality and length to **tpdc** but which contains organocatalytic squaramide centers. Therefore, the four MOFs share the same organocatalytic squaramide moiety, but confine it within distinct pore environments. We then evaluated these MOFs as heterogeneous H-bonding catalysts in organic transformations: a Friedel-Crafts alkylation and an epoxide ring-opening. Some of them exhibited good performance in both reactions but all showed distinct catalytic profiles that reflect their structural differences.

1. Introduction

Metal-organic frameworks (MOFs) are crystalline porous compounds based on metal ions or clusters connected by organic ligands, whose topology, pore size and/or chemical composition can be modulated to achieve functionalities such as catalysis or adsorption. Those MOFs that exhibit confinement effects, and pores functionalized with specific and highly-localized catalytic sites, are a potentially limitless source of new heterogeneous catalysts. Most reported MOF-based catalysts have been designed around metallic catalytic sites. In these, coordinatively unsaturated metal sites form the MOF structure itself, or metal ions/complexes/clusters/nanoparticles are encapsulated within the MOF pores or connected to the MOF organic linkers.[1–3]

An alternative, less-explored approach to synthesizing heterogeneous MOF catalysts is to incorporate organocatalytic centers within MOFs.[4,5] This can be done via post-synthetic modifications of the organic linkers in existing MOFs[6–10], or during MOF synthesis, by using organic linkers that contain these organocatalytic centers.[11–25] The latter approach in particular can benefit from reticular chemistry, which can facilitate rational design of MOF-based catalysts with pre-defined framework topologies and pores. Indeed, as Prof. O. M. Yaghi has affirmed, an important feature of reticular chemistry is that "for a given framework, the constituents can also be chemically functionalized either pre- or post-synthetically, while maintaining the framework's connectivity, to produce functionalized pores."[26,27] In our field, this idea translates to the ability to modify the organic linker of an existing MOF by inserting an organocatalytic center, *without* modifying the linker length or topology, thus enabling synthesis of the corresponding isoreticular MOF structure containing the desired center.

Siu *et al.* were among the first to prepare an iconic MOF-based catalyst by this organocatalytic-center approach: the isoreticular NH_2-MIL-101, which showed high activity in

base-catalyzed Knoevenagel condensations.[20] Soon afterwards, Hupp *et al.* similarly introduced H-bonding organocatalytic centers (*e.g.* urea and squaramide) into programmable MOFs.[21–23] For example, they synthesized two isoreticular UiO-67 catalysts from biphenyl-4,4'-dicarboxylate linkers functionalized with pendant urea and squaramide groups.[21,23] This type of strategy has since been extended to many other isoreticular MOF-based catalysts containing urea moieties. [17–19,21,22]

Herein we report the rational synthesis of four heterogeneous, MOF-based catalysts with programmable topologies, based on use of reticular chemistry and on MOF 3D-structural information from the Cambridge Structural Database.[28] Briefly, we confined the same squaramide organocatalytic center into different MOFs that exhibit distinct nanoscale-pore environments. A squaramide was chosen as the test case organocatalyst because it is known that its immobilization into a framework enhances its reactivity and stability while avoiding any self-quenching phenomena due to their tendency to self-aggregate in solution.[4,29] The MOFs are isoreticular versions of **pcu-IRMOF-16**, **fcu-UiO-68** and **pillared-pcu-SNU-8X**, the three most common topologies of MOFs built from the organic linker *p*,*p*'-terphenyldicarboxylic acid (**tpdc**). Our four-step strategy (Figure 1) entailed the design and synthesis of a new linker, 3,4-dioxocyclobut-1-ene-1,2-diyl)bis(azanedyil)-*p*-dibenzoic acid) (**Sq_tpdc**), which is identical in directionality and length to **tpdc** but which contains organocatalytic squaramide centers. We evaluated the four MOF-based catalysts for H-bonding catalysis in a representative Friedel-Crafts alkylation and a representative epoxide ring-opening. Some of these MOFs exhibited good performance in both reactions but all showed distinct catalytic profiles that reflect their structural differences.

- Insert Figure 1-

2. Experimental section.

2.1 Materials and methods

Zinc(II) nitrate hexahydrate, zirconium(IV) oxychloride, 4,4'-bipyridyne and 2,5-bispyridylethane, dimethyl squarate, 4-aminobenzoic acid, trimethylamine, anilines were purchased from commercial sources and used as received without further purification. *4,4'-(3,4-dioxocyclobut-1-ene-1,2-diyl)bis(azanediyl))dibenzene* used as molecular catalyst (MC) was synthesized following a described procedure in the literature.[25]

NMR spectra were acquired on a Bruker Avance 300 MHz spectrometer, running at 300 MHz (^{1}H) or 75 MHz (^{13}C). In some cases (noted), they were acquired on a Bruker Avance 250 MHz spectrometer. Chemical shifts (δ) are reported in ppm relative to residual solvent signals ($CDCl_3$: 7.26 ppm for ^{1}H-NMR and 77.16 ppm for ^{13}C-NMR; DMSO-d_6: 2.50 ppm for ^{1}H-NMR and 39.52 ppm for ^{13}C-NMR). Coupling constants are reported in Hertz. The following abbreviations are used to describe peak patterns: s (singlet), d (doublet), t (triplet), q (quartet), m (multiplet), bs (broad singlet). Different methods were used for measuring the exact mass (indicated for each case). MS (ESI) (Electrospray mass spectroscopy) spectra were acquired with an Agilent Technologies 6120 Quadrupole LC/MS. MS (EI) (Electron Ionization Mass Spectroscopy) spectra were acquired with an Agilent Technologies 5977B MSD. For both techniques, MassWorks v. 4.0.0.0 (Cerno Bioscience) was used for the formula identification. MassWorks is MS-calibration software that calibrates for isotope profile as well as for mass accuracy, enabling highly accurate comparisons between calibrated and theoretical spectra. MS (TOF-ESI) (Electrospray Mass Spectroscopy with Time-of-Flight detector) spectra were acquired with microTOF-Q Bruker Daltonics spectrometer. Optical rotation was recorded in cells with 10-cm path-length; the solvents

and concentrations (in g/100 mL) are indicated in each case. Flash chromatography was performed on silica-gel columns (40 μm to 63 μm; pore size: 60 Å). Kinetics were studied by monitored reaction progress by gas chromatography using a 7820A GC System (Agilent Technologies) equipped with a Flame Ionization Detector (FID). Elemental analyses were obtained on a EA1108 micro-analyzer (CarboErba). Volumetric N_2 adsorption–desorption isotherms were collected at 77 K using an ASAP2020 HD (Micromeritics).

2.2. X-Ray Diffraction.

Composition of all bulk materials was confirmed through X-Ray powder diffraction (XRPD) measurements were collected on an X'Pert PRO MPD analytical diffractometer (Panalytical) at 45 kV and 40 mA using Cu Kα radiation (λ= 1.5419 Å) and compared with single-crystal simulated patterns. Single-Crystal X-Ray Diffraction (SCXRD) data on **Sq_IRMOF-16**, **Sq_UiO-68,** **Sq_SNU-8X** and **Sq_bptMOF** were collected at 100(2) K in the BL13-XALOC beamline[30] at the ALBA synchrotron, on a single-axis goniometer with a Pilatus 6M detector using a monochromatic X-ray beam (λ = 0.82656 Å). The data frames were integrated and scaled using XDS software.[31] Absorption correction was not applied. All structures were solved by direct methods and subsequently refined by correction of F2 against all reflections, using SHELXT2013 and SHELXL2013 within the WinGX package.[32] They contain some disorder molecules. Attempts to adequately model the disordered molecules were unsatisfactory; therefore, the PLATON/SQUEEZE routine was applied to mask out the disordered electron density.[33]

2.3. Synthesis of 4-((2-methoxy-3,4-dioxocyclobut-1-en-1-yl)amino)benzoic acid.

A white suspension of dimethyl squarate (1.00 gr, 7.00 mmol) and 4-aminobenzoic acid (0.960 g, 7.00 mmol) in 20 mL of dry MeOH was stirred 24 hours at room temperature. The resulting yellow

suspension was filtered, washed with MeOH and Et_2O, and then dried under vacuum to afford the desired pure compound 4-((2-methoxy-3,4-dioxocyclobut-1-en-1-yl)amino)benzoic acid (1.30 g, 75% yield). 1 H-NMR (300 MHz, DMSO-d6): δ 12.71 (bs, 1H), 10.96 (s, 1H), 7.94 – 7.86 (m, 2H), 7.50 – 7.40 (m, 2H), 4.40 (s, 3H). 13C-NMR (75 MHz, DMSO-d6): δ 187.6, 184.4, 179.5, 169.1, 166.8, 142.0, 130.6, 125.7, 118.7, 60.7.

2.4. Synthesis of 4,4'-((3,4-dioxocyclobut-1-ene-1,2-diyl)bis(azanediyl))dibenzoic acid (Sq_tpdc).

A mixture of 4-((2-methoxy-3,4-dioxocyclobut-1-en-1-yl)amino)benzoic acid (0.90 gr, 3.60 mmol), 4-aminobenzoic acid b (0.497 g, 3.60 mmol) and Et_3N (0.503 mL, 3.60 mmol) in 18 mL of dry CH_3CN in a sealed tube was heated at 80 ºC for 24 hours. The resulting suspension was concentrated down to *ca.* 9 mL. Then, H_2O (20 mL) was added, and the pH was adjusted to 1 (conc. HCl). The solid was filtered and washed thoroughly with H_2O until neutral pH, washed with Et_2O and finally, and dried under vacuum to afford pure squaramide **Sq_tpdc** (1.01 g, 80% yield). 1 H-NMR (250 MHz, DMSO-d6): δ 12.72 (bs, 2H), 10.31 (bs, 2H), 7.94 (d, J = 8.4 Hz, 4H), 7.57 (d, J = 8.4 Hz, 4H). 13CNMR (63 MHz, DMSO-d6): δ 182.0, 166.8, 165.9, 142.4, 130.9, 125.1, 118.0. MS (TOF-ESI-): Calculated for $C_{18}H_{11}N_2O_6$ - [M-H] -: 351.0623. Found: 351.0614.

2.5. Synthesis of Sq_IRMOF-16.

$Zn(NO_3)_2 \cdot 6H_2O$ (0.017 g, 0.057 mmol) and **Sq_tpdc** (0.020 g, 0.057 mmol) were dissolved in 4.8 mL DMF and heated to 85 ºC for 7 days. This afforded yellow cubic crystals (0.010 g; 53% yield), which were stored in DMF. FT-IR (ATR; cm^{-1}): 1650 (C=O from carboxylate) selected band. Anal. Calcd. for ($[Zn_4O(L_1)_3] \cdot 6H_2O \cdot 4DMF$; $Zn_4C_{66}H_{70}N_{10}O_{29}$): C, 45.85; H, 4.08; N, 8.10, found: C, 45.23; H, 3,97; N, 8.34

2.6. Synthesis of the Sq_UiO-68.

To a DMF solution (4 mL) of **Sq_tpdc** (20 mg, 0.057 mmol), $ZrOCl_2 \cdot 8H_2O$ (18.31 mg, 0.057 mmol) were added 5 mL of a DMF/formic acid mixture (4:1 w/w). The mixture was heated at 120 °C for 1 week. This afforded yellow crystals, which were filtered, washed with DMF and MeOH, and then, air-dried to give **Sq_UiO-68** (22.3 mg; 14 %). Elemental analysis for **Sq_UiO-68** - $[Zr_6(OH)_4(\mathbf{1})_6]$, calculated (%): C: 47.74, H: 2.37, N: 6.19; found: C: 46.9, H: 2.88 N: 6.31; FT-IR (ATR; cm^{-1}, selected bands): 3167 (OH); 2927 (NH); 1793, 1647 (C=O from DMF); 1597 (C=O from carboxylate). Anal. Calcd. for ($[Zr_6O_4(OH)_4(L_1)_6]$; $Zr_6C_{108}H_{70}N_{12}O_{44}$): C, 46.54; H, 2.53; N, 6.03, found: C, 47.12; H, 2,58; N, 7,00.

2.7. Synthesis of Sq_SNU-8X.

$Zn(NO_3)_2 \cdot 6H_2O$ (0.017 g, 0.057 mmol), **Sq_tpdc** (0.020 g, 0.057 mmol) and 4,4'-bipyridine (0.009 g, 0.057 mmol) were dissolved in 4.8 mL DMF. The mixture was placed in a 10-mL Erlenmeyer flask, which was covered with a septum, and then heated to 85 ºC for 5 days. This afforded yellow crystals (0.015 g; 56% yield). FT-IR (ATR; cm^{-1}, selected bands): 3200 (OH), 1788, 1639, 1598 (C=O from carboxylate), 1558, 1488, 1367, 1240, 1180, 1100, 777, 636, 475. Anal. Calcd for $Zn_2C_{55}H_{49}N_9O_{15}$: C, 54.74; H, 4.09; N, 10.45, found: C, 54.30; H, 3.94; N, 10.60.

2.8. Synthesis of Sq_BptMOF.

$Zn(NO_3)_2 \cdot 6H_2O$ (0.017 g, 0.057 mmol), **Sq_tpdc** (0.020 g, 0.057 mmol) and 1,2-Bis(4-pyridyl)ethane (0.010 g, 0.057 mmol) were dissolved in 4.8 mL DMF. The mixture was placed in a 10-mL Erlenmeyer flask, which was covered with a septum, and then heated to 85 ºC for 5 days. This afforded orange crystals (0.013 g; 45% yield). FT-IR (ATR; cm^{-1}, selected bands): 3200

(OH), 1787, 1703, 1644 (C=O from carboxylate), 1602, 1543, 1493, 1440, 1241, 1177, 1102, 775. Anal. Calcd for $Zn_2C_{54}H_{54}N_8O_{18}$: C, 52.57; H, 4.41; N, 9.08, found: C, 52.00; H, 4.16; N, 9.20.

2.9. Catalysis experiments.

A 0.005 mmol-aliquot of a single, dried MOF-based catalyst (2.8 mg of **Sq_IRMOF-16**; 2.9 mg of **Sq_SNU-8X**; 2.9 mg of **Sq_BptMOF**; or 2.4 mg of **Sq_UiO-68**), 0.1 mmol of *p*-methoxyaniline and a stirring bar were transferred to a septum-sealed vial, which was flushed with N_2 for 15 minutes. Note that **Sq_SNU-8X**, **Sq_BptMOF**, and **Sq_UiO-68** were incubated in methanol for 72 hours before use. Then, 200 μL of ethyl epoxide was added to the mixture. The mixture was heated to 60 °C and stirred for 8 hours. At different time-points (1h, 2h, 4h, 6h and 8h), a 20-μL aliquot of the reaction mixture was removed, and then diluted with 500 μL of a 0.005 M solution of 2-methylnaphthalene (gas chromatography standard) in toluene. The resulting sample was then analyzed by gas chromatography with FID.

3. Results and Discussion.

3.1. Design, synthesis and analysis of the squaramide-based linker

We designed the linker **Sq_tpdc** by attaching two benzoic acid moieties to the NH groups of the squaramide (Figure 1), which we justified based on two factors. Firstly, we reasoned that the phenyl rings would favor structural planarity and rigidity in the linker, while the two opposing carboxylic groups would enable construction of extended structures *via* metal ion coordination. Secondly, we sought to exploit the *para* position of squaramide groups relative to the carboxyl groups, to maximize the acidity of the squaramide-NH protons. Specifically, the electron-

withdrawing nature of the carboxylic groups acts by resonance in the *ortho* and *para* positions, thereby diminishing the electron density of the NH groups and increasing their acidity and, consequently, their ability to form hydrogen bonds (*i.e.* to catalyze H-bonding reactions). We further reasoned that since the squaramide ring is roughly equivalent in size to a phenyl ring, then the carboxylic groups of **Sq_tpdc** would be separated by a distance very close to that corresponding to three phenyl rings. Accordingly, we considered that **Sq_tpdc** is roughly equivalent in both directionality (topology) and length to **tpdc** (Figure 1), a well-known dicarboxylate linker in MOF synthesis.[34–36] Once we had designed **Sq_tpdc,** we synthesized it by a previously-reported, two-step method.[25]

3.2. Cambridge Structural Database search

We searched the Cambridge Crystallographic Data Centre (CCDC) database (ConQuest v. 2.0.0, CCDC, Cambridge, UK) for 3D MOF structures built from **tpdc**. We found three structures, which we classified into two framework topologies: two of the structures corresponded to **IRMOF-16** MOF (**pcu** topology; one non-interpenetrated framework and one double-interpenetrated framework; Figure 2a); and the third one, to **UiO-68** MOF (**fcu** topology; Figure 2b). The **pcu-IRMOF-16** comprises Zn_4O clusters linked to six **tpdc** linkers in an octahedral coordination. The non-interpenetrated **IRMOF-16** contains cubic cavities delimited by twelve **tpdc** linkers, with a pore opening of *ca.* 15 Å.[36] The **fcu-UiO-68** comprises octahedral $[Zr_6O_4(OH)_4]$ clusters linked by twelve **tpdc** linkers that create two types of spaces between them: *octahedral cavities* delimited by twelve **tpdc** linkers, and *tetrahedral cavities* delimited by six **tpdc** linkers, both showing trigonal pore openings of *ca.* 10 Å.[34,35]

- **Insert Figure 2-**

To extend the number of potential 3D MOF structures that could be synthesized using **Sq_tpdc**, we also searched for 3D MOF structures built from **tpdc** functionalized at any of the four aromatic positions of the central phenyl ring by groups that cannot coordinate to metal ions (*i.e.* to maintain the directionality of the parent **tpdc)**. This revealed 53 additional 3D structures: fifteen (28%) of which exhibit ***fcu*** topology and six (11%) of which, ***pcu*** topology.[37–50] Of the remaining 32 structures, eighteen (24%) correspond to **pillared-*pcu*** MOFs (Figure 2c,d).[51–55] In these latter MOFs, paddle-wheel M_2 [M = Zn(II), Cu(II) and Cd(II)] clusters are bridged by four **tpdc** linkers that form 2D square grids, which are linked by pillared N-based linkers that form 3D structures with bidirectional 1D pores. These pores are delimited by four **tpdc** linkers and by two **tpdc** and two pillared linkers. In some cases, the pillared linkers are not truly perpendicular to the cluster-carboxylic layers and the pores are distorted prisms with rhombic windows. The fourteen remaining structures pertain to four MOF topology groups: eight (15%) of them comprise *planes or chains* of metal oxides [M = Co(II), Ni(II), Mn(II), Pb(II), Mg(II), Eu(III) and Cd(II)] linked by **tpdc** linkers; three (6%) of them exhibit a ***diamond*** topology; two (4%) of them, ***acs*** topology;[56,57]and one (2%) of them, ***bcu*** topology.[37] The ***diamond*** MOFs are formed by linkage of tetrahedral Zn(II) or Cd(II) ions through two **tpdc** and two N,N'-based linkers. The ***acs*** MOFs are formed through linkage of trigonal M_3O (M= Fe(III) and In(III)] clusters by six **tpdc** linkers (two linkers per edge). Both structures show pores with the shape of a bipyramidal trigonal base (or a slightly distorted tetrahedron) delimited by six **tpdc** ligands with (slightly distorted) hexagonal windows of *ca.* 19 Å. The ***bcu*** MOF is formed by octahedral [$Zr_6O_8(OH_2)_8$] clusters

coordinated by eight **tpdc** linkers that generate octahedral pores, which are delimited by eight **tpdc** linkers and exhibit rhombic windows of *ca.* 13 Å.

3.3. Selection, synthesis and structural analysis of isoreticular MOFs

After the Cambridge Structural Database search, we selected the three most common MOF topologies and investigated the synthesis of the corresponding isoreticular MOFs incorporating the squaramide moieties. Here, we chose both ***pcu*** **IRMOF-16** and ***fcu*** **UiO-68** frameworks (Figure 2a,b), as they are the only two topologies reported using the non-functionalized **tpdc** linker and are highly abundant, together corresponding to 41% of all reported 3D structures. We also chose **pillared-*pcu*** MOFs (Figure 2c,d), given their rich potential for obtaining myriad compositions by simply exchanging the pillared linker, and because they, too, are highly abundant (32% of all reported 3D structures). Here, we used **bipy** and **bpt** linkers as the pillars, aiming to synthesize isoreticular versions of **SNU-8X** (hereafter, ***Sq_SNU-8X***) and **OZASUF** (hereafter, ***Sq_bptMOF***).

Characterization of the synthesized **Sq_IRMOF-16** crystals by SCXRD confirmed that they retain the characteristic **IRMOF-16** ***pcu*** topology (Figure 2a). Thus, **Sq_IRMOF-16** exhibits a 3D structure built from the connection of Zn_4O clusters through six **Sq_tpdc** linkers to form the expected cubic cavities delimited by twelve **Sq_tpdc** linkers and showing a pore opening of 14 Å (Figure 1a; Brunauer-Emmett-Teller surface area S_{BET} measured by N_2 sorption at 77 K of 784 m^2/g.). However, in this structure, the squaramide rings of the **Sq_tdpc** linkers exhibit high mobility and positional disorder: they could not be positioned even when SCXRD was performed at 100 K. Accordingly, their position and orientation were determined by employing rigid-body restraints, which revealed that **Sq_IRMOF-16** has cubic cavities containing zero, four or eight squaramide rings pointing towards them (Figure 2a). However, given the high mobility of the

squaramide rings, each cubic cavity could also be statistically considered to contain three rings pointing towards it.

Characterization of the synthesized **Sq_UiO-68** crystals by SCXRD confirmed formation of the desired analogous ***pcu*** **UiO-68** structure (Figure 2b), in which the squaramide moieties of the **Sq-tpdc** linkers were fitted in electron-density maps, by considering them as rigid bodies. Overall, **Sq_UiO-68** exhibits a ***fcu*** topology in which $[Zr_6O_4(OH)_4]$ nodes are connected *via* 12 **Sq_tpdc** ligands forming a porous network (S_{BET} = 637 m^2/g). This network shows octahedral cavities and tetrahedral cavities delimited by twelve and six **Sq_tpdc** linkers, respectively, and connected by windows of 7 Å. In these cavities, six squaramide rings are pointing towards the octahedron cavities (Figure 2b).

Similarly to the previous examples, SCXRD of the synthesized **Sq_SNU-8X** crystals revealed formation of the expected pillared **MOF** with **pcu** topology (Figure 2). The basic **Sq_SNU-8X** units are paddle-wheel Zn_2 clusters, in which each Zn(II) ion exhibits square-pyramidal coordination geometry. The equatorial sites of the pyramid are occupied by four oxygen atoms of the carboxylate groups of four **Sq_tpdc** linkers, whereas the last axial coordination position is occupied by a nitrogen atom of the N-donor **bipy** linker. The resulting paddle-wheel Zn_2 clusters are connected through four **Sq_tpdc** linkers that form 2D square grids, which in turn are connected by **bipy** linkers that form 3D **pcu** nets, which are doubly interpenetrated. Note that the parent **SNU-8X** is also a doubly-interpenetrated MOF. Interpenetrated **Sq_SNU-8X** possesses 1D channels of two sizes: 12 Å x 12 Å, delimited by four **Sq_tpdc** and running along the *a*-axis; and 8 Å x 12 Å, delimited by two **Sq_tpdc** and two **bipy** linkers and running along the *c*-axis (Figure 2c). The squaramide rings are parallel to the pores along the *a*-axis but point towards those

along the *c*-axis. Based on these apparent voids and free channels, the porosity of **Sq_SNU-8X** was evaluated by measuring its N_2 sorption at 77 K, which gave an S_{BET} value of 634 m^2/g.

Finally, we prepared **Sq_bptMOF** by using the same conditions as for **Sq_SNU-8X**, except that instead of **bipy**, we used **bpt**. Interestingly, SCXRD revealed formation of a double-interpenetrated pillared **pcu** MOF (S_{BET} = 789 m^2/g) much like that in **Sq_SNU-8X**, as it similarly contained 1D channels of two sizes: 8 Å x 11 Å, delimited by two **Sq_tpdc** and two **bipy** linkers and running along the *a*-axis; and 12 Å x 11 Å, delimited by four **Sq_tpdc** linkers and running along the *c*-axis (Figure 2d). In this case, the squaramide rings point towards the pores along the *a*-axis but are parallel to those along the *c*-axis.

3.4. Evaluation of catalytic performance

We hypothesized that synthesis of diverse heterogeneous catalysts using our reticular approach, followed by catalytic screening of them in test reactions, would greatly augment the probability of finding high-performing catalysts for any desired chemistry. Thus, we evaluated our MOF-based catalysts in two archetypical, squaramide-catalyzed reactions: a representative Friedel-Crafts alkylation and a representative epoxide ring-opening. Importantly, XRPD performed during and after these two catalytic reactions confirmed the stability of all squaramide-based MOFs (see S.I., Figure SXX). Their stability was further corroborated by discarding the leaching of catalytic species into the reaction media. Such feature was assessed by means of experiments consisting on filtering off the catalytic material at intermediate stages of the each reaction observing that product content did not evolve further after MOF removal. Crucially, when the molecular squaramide *4,4'-(3,4-dioxocyclobut-1-ene-1,2-diyl)bis(azanediyl))dibenzene* (C) was used alone as catalyst, both reactions barely progressed, likely due to its self-aggregation and poor solubility. This result

supported our original strategy of designing heterogeneous catalysts in which the squaramide rings are immobilized within MOFs.

We then studied the kinetics of a representative Friedel-Crafts alkylation: reaction of indole (0.15 mmol) and β-nitrostyrene (0.10 mmol) in the presence of the corresponding squaramide-based MOFs (0.005 mmol = 5 mol% [catalytic centers] relative to β-nitrostyrene) at 60 ºC. Figure 3 is a plot of the kinetics for each squaramide-based MOF catalyst over 72 hours. The most active catalyst for this reaction was **Sq_SNU-8X** (yield: 85%) followed by **Sq_UiO-68** and **Sq-IRMOF-16** (yield for each: *ca.* 70%), and finally, **Sq_bptMOF** (yield: 18%). We attributed the low performance of **Sq_bptMOF** to the structural flexibility commonly observed when flexible pillar ligands such as **bpt**, which have a high degree of rotation freedom due to the $–CH_2$-CH_2- chain between the pyridine fragments, are used to synthesize pillared **fcu** MOFs.[9] This highly dynamic behavior impedes catalytic performance, as it decreases the pore size and therefore accessibility of the substrates to the active sites.

- **Insert Figure 3 –**

We next studied the kinetics of a representative epoxide ring-opening: reaction of 4-methoxy aniline (0.1 mmol) and ethyl epoxide (molar excess) at 60 °C in the presence of the corresponding squaramide-based MOF (0.005 mmol = 5 mol% [catalytic centers] relative to 4-methoxy aniline) for 8 hours. Figure 4 shows the kinetics of the ring-opening reaction. This reaction can consecutively generate two products: the mono-addition and bis-addition products. The best catalysts for the formation of the bis-addition product were **Sq_IRMOF-16** and **Sq_SNU-8X**, which gave nearly quantitative transformation after 8 hours. In contrast, **Sq_UiO-68** and

Sq_bptMOF gave roughly 50/50 mixtures of the mono- addition and bis-addition products after 8 hours.

- **Insert Figure 4-**

We explained this discrepancy in catalytic performance according to sterics. Specifically, formation of the bis-adduct from the double epoxide ring-opening process appears to be highly sterically demanding and sensitive to aperture sizes. Accordingly, the most sterically-restricted MOFs would be the worse catalysts for the double-epoxide activation. This was indeed the case for the flexible **Sq_bptMOF** (*vide supra*) as well as for **Sq_UiO-68**, which has a smaller pore opening (7 Å) than do **Sq_IRMOF-16** (14 Å) and **Sq_SNU-8X** (12 Å).

4. Conclusions.

In summary, we have reported the design, synthesis and testing of heterogeneous, MOF-based catalysts containing squaramide organocatalysts trapped within their pores. We demonstrated that organocatalytic MOFs with programmable topologies can be synthesized by exploiting reticular chemistry and 3D MOF-structural data from the Cambridge Structural Database. Our approach entailed design and synthesis of a new dicarboxylate linker containing the squaramide ring, **Sq_tpdc**, which we the used to prepare four MOF-based catalysts that share the same organocatalytic center but differ in their pore environments. The MOFs are isoreticular versions of **pcu-IRMOF-16**, **fcu-UiO-68** and **pillared-pcu-SNU-8X**, the three most common topologies of MOFs built from the organic linker *p*,*p*'-terphenyldicarboxylic acid (**tpdc**), which is similar in length and directionality to **Sq_tpdc**. **Sq_SNU-8X** was the best catalyst in a

representative Friedel-Crafts alkylation, whereas **Sq_IRMOF-16** and **Sq_SNU-8X** were the best in a representative epoxide ring-opening (formation of the bis-addition product). Using an approach like ours, researchers could ultimately design an entire catalog of MOF-based catalysts, thereby greatly increasing the chances of finding high-performance catalysts for targeted chemistries.

Acknowledgments

This work was supported by the Spanish MINECO (projects RTI2018-095622-B-I00 and CTQ2015-64561-R), the Catalan AGAUR (project 2017 SGR 238), the ERC under the EU FP7 (ERC−Co 615954), and European Union's Horizon 2020 research and innovation program, under grant agreement No 685727, and European Structural Funds (S2018/NMT-4367). It was also funded by the CERCA Program/Generalitat de Catalunya. ICN2 is supported by the Severo Ochoa program from the Spanish MINECO (Grant No. SEV-2017-0706).

Electronic Supplementary Material: Supplementary Material (XXXXXXXX) is available in the online version of this article at https://XX.

Address correspondence to Inhar Imaz, inhar.imaz@icn2.cat; Rubén Mas-Ballesté, ruben.mas@uam.es; José Alemán, jose.aleman@uam.es; Daniel Maspoch, daniel.maspoch@icn2.cat

References

1 Y. B. Huang, J. Liang, X. S. Wang and R. Cao, *Chem. Soc. Rev.*, 2017, **46**, 126–157.
2 A. Dhakshinamoorthy, Z. Li and H. Garcia, *Chem. Soc. Rev.*, 2018, **47**, 8134–8172.
3 J. Liu, L. Chen, H. Cui, J. Zhang, L. Zhang and C. Y. Su, *Chem. Soc. Rev.*, 2014, **43**, 6011–6061.
4 J. V. Alegre-Requena, E. Marqués-López, R. P. Herrera and D. D. Díaz, *CrystEngComm*, 2016, **18**, 3985–3995.
5 S. Mandal and P. C. Rao, *Chem. – An Asian J.*, 2019, **X**, doi.org/10.1002/asia.201900823.
6 X. W. Dong, T. Liu, Y. Z. Hu, X. Y. Liu and C. M. Che, *Chem. Commun.*, 2013, **49**, 7681–7683.
7 Y. Luan, N. Zheng, Y. Qi, J. Tang and G. Wang, *Catal. Sci. Technol.*, 2014, **4**, 925–929.
8 S. J. Garibay, Z. Wang and S. M. Cohen, *Inorg. Chem.*, 2010, **49**, 8086–8091.
9 Y. Zang, J. Shi, F. Zhang, Y. Zhong and W. Zhu, *Catal. Sci. Technol.*, 2013, **3**, 2044–2049.
10 S. Aguado, J. Canivet, Y. Schuurman and D. Farrusseng, *J. Catal.*, 2011, **284**, 207–214.
11 X. Zhang, Z. Zhang, J. Boissonnault and S. M. Cohen, *Chem. Commun.*, 2016, **52**, 8585–8588.
12 S. M. Cohen, Z. Zhang and J. A. Boissonnault, *Inorg. Chem.*, 2016, **55**, 7281–7290.
13 A. A. Tehrani, S. Abedi, A. Morsali, J. Wang and P. C. Junk, *J. Mater. Chem. A*, 2015, **3**, 20408–20415.
14 P. C. Rao and S. Mandal, *ChemCatChem*, 2017, **9**, 1172–1176.
15 E. A. Hall, L. R. Redfern, M. H. Wang and K. A. Scheidt, *ACS Catal.*, 2016, **6**, 3248–3252.
16 D. Markad and S. K. Mandal, *ACS Catal.*, 2019, **9**, 3165–3173.
17 Z. Ju, S. Yan and D. Yuan, *Chem. Mater.*, 2016, **28**, 2000–2010.
18 H. Zhang, X. W. Gao, L. Wang, X. Zhao, Q. Y. Li and X. J. Wang, *CrystEngComm*, 2019, **21**, 1358–1362.
19 X. J. Wang, J. Li, Q. Y. Li, P. Z. Li, H. Lu, Q. Lao, R. Ni, Y. Shi and Y. Zhao, *CrystEngComm*, 2015, **17**, 4632–4636.
20 P. Serra-Crespo, E. V. Ramos-Fernandez, J. Gascon and F. Kapteijn, *Chem. Mater.*, 2011, **23**, 2565–2572.
21 P. W. Siu, Z. J. Brown, O. K. Farha, J. T. Hupp and K. A. Scheidt, *Chem. Commun.*, 2013, **49**, 10920–10922.
22 J. Roberts, B. Fini, A. Sarjeant, O. Farha, J. Hupp and K. Scheidt, *J. Am. Chem. Soc.*, 2012, **134**, 3334–3337.
23 C. M. McGuirk, M. J. Katz, C. L. Stern, A. A. Sarjeant, J. T. Hupp, O. K. Farha and C. A. Mirkin, *J. Am. Chem. Soc.*, 2015, **137**, 919–925.
24 D. J. Lun, G. I. N. Waterhouse and S. G. Telfer, *J. Am. Chem. Soc.*, 2011, **133**, 5806–5809.
25 C. Vignatti, J. Luis-Barrera, V. Guillerm, I. Imaz, R. Mas-Ballesté, J. Alemán and D. Maspoch, *ChemCatChem*, 2018, **10**, 3995–3998.
26 O. M. Yaghi, *ACS Cent. Sci.*, 2019, **5**, 1295–1300.
27 O. M. Yaghi, *Mol. Front. J.*, 2019, **3**, 66–83.
28 M. P. L. and S. C. W. C. R. Groom, I. J. Bruno, *Acta Cryst.*, 2016, **B72**, 171–179.
29 R. Ian Storer, C. Aciro and L. H. Jones, *Chem. Soc. Rev.*, 2011, **40**, 2330.
30 S. F. and J. B. J. Juanhuix, F. Gil-Ortiz, G. Cuni, C. Colldelram, J. Nicolas, J. Lidon, E. Boter, C. Ruget, *J. Synchr. Rad.*, 2014, **21**, 679.
31 W. Kabsch, *Acta Crystallogr. Sect. D*, 2010, 66, 125.
32 G. Sheldrick, *Acta Crystallogr. Sect. A*, 2015, **71**, 3.
33 G. Sheldrick, *Acta Crystallogr. Sect. C*, 2015, **71**, 3.
34 K. Manna, P. Ji, Z. Lin, F. X. Greene, A. Urban, N. C. Thacker and W. Lin, *Nat. Commun.*, 2016, **7**, 1–11.
35 A. Schaate, P. Roy, A. Godt, J. Lippke, F. Waltz, M. Wiebcke and P. Behrens, *Chem. Eur. J.*, 2011, **17**, 6643–6651.
36 M. Eddaoudi, J. Kim, N. Rosi, D. Vodak, J. Wachter, M. O'Keeffe and O. M. Yaghi, *Science*, 2002,

295, 469–472.
37 M. Carboni, Z. Lin, C. W. Abney, T. Zhang and W. Lin, *Chem. Eur. J.*, 2014, **20**, 14965–14970.
38 Y. A. Li, S. Yang, Q. Y. Li, J. P. Ma, S. Zhang and Y. Bin Dong, *Inorg. Chem.*, 2017, **56**, 13241–13248.
39 K. Manna, T. Zhang, M. Carboni, C. W. Abney and W. Lin, *J. Am. Chem. Soc.*, 2014, **136**, 13182–13185.
40 E. A. Dolgopolova, O. A. Ejegbavwo, C. R. Martin, M. D. Smith, W. Setyawan, S. G. Karakalos, C. H. Henager, H. C. Zur Loye and N. B. Shustova, *J. Am. Chem. Soc.*, 2017, **139**, 16852–16861.
41 Y. He, Y. L. Hou, Y. L. Wong, R. Xiao, M. Q. Li, Z. Hao, J. Huang, L. Wang, M. Zeller, J. He and Z. Xu, *J. Mater. Chem. A*, 2018, **6**, 1648–1654.
42 B. Li, B. Gui, G. Hu, D. Yuan and C. Wang, *Inorg. Chem.*, 2015, **54**, 5139–5141.
43 H. Huang, H. Sato and T. Aida, *J. Am. Chem. Soc.*, 2017, **139**, 8784–8787.
44 G. E. M. Schukraft, S. Ayala, B. L. Dick and S. M. Cohen, *Chem. Commun.*, 2017, **53**, 10684–10687.
45 H. L. Jiang, D. Feng, T. F. Liu, J. R. Li and H. C. Zhou, *J. Am. Chem. Soc.*, 2012, **134**, 14690–14693.
46 B. Gui, X. Meng, Y. Chen, J. Tian, G. Liu, C. Shen, M. Zeller, D. Yuan and C. Wang, *Chem. Mater.*, 2015, **27**, 6426–6431.
47 T. Y. Luo, C. Liu, S. V. Eliseeva, P. F. Muldoon, S. Petoud and N. L. Rosi, *J. Am. Chem. Soc.*, 2017, **139**, 9333–9340.
48 R. Wang, M. Zhang, X. Liu, L. Zhang, Z. Kang, W. Wang, X. Wang, F. Dai and D. Sun, *Inorg. Chem.*, 2015, **54**, 6084–6086.
49 K. Oisaki, Q. Li, H. Furukawa, A. U. Czaja and O. M. Yaghi, *J. Am. Chem. Soc.*, 2010, **132**, 9262–9264.
50 V. A. Online, L. Liu, X. Wang, Q. Zhang, Q. Li and Y. Zhao, 2013, **13**, 841–844.
51 C. Zhang, H. Hao, Z. Shi and H. Zheng, *CrystEngComm*, 2014, **16**, 5662–5671.
52 J. Sahu, M. Ahmad and P. K. Bharadwaj, *Cryst. Growth Des.*, 2013, **13**, 2618–2627.
53 T. K. Prasad and M. Paik, *Chem. - An Asian J.*, 2015, **10**, 2257–2263.
54 I. M. Hauptvogel, R. Biedermann, N. Klein, I. Senkovska, A. Cadiau, D. Wallacher, R. Feyerherm and S. Kaskel, *Inorg. Chem.*, 2011, **50**, 8367–8374.
55 J. Sahu, A. Aijaz, Q. Xu and P. K. Bharadwaj, *Inorg. Chim. Acta*, 2015, **430**, 193–198.
56 X. Liu, B. Liu, G. Li and Y. Liu, *J. Mater. Chem. A*, 2018, **6**, 17177–17185.
57 D. Feng, K. Wang, Z. Wei, Y. P. Chen, C. M. Simon, R. K. Arvapally, R. L. Martin, M. Bosch, T. F. Liu, S. Fordham, D. Yuan, M. A. Omary, M. Haranczyk, B. Smit and H. C. Zhou, *Nat. Commun.*, 2014, **5**, 5723.

Broto et al., Figure 1

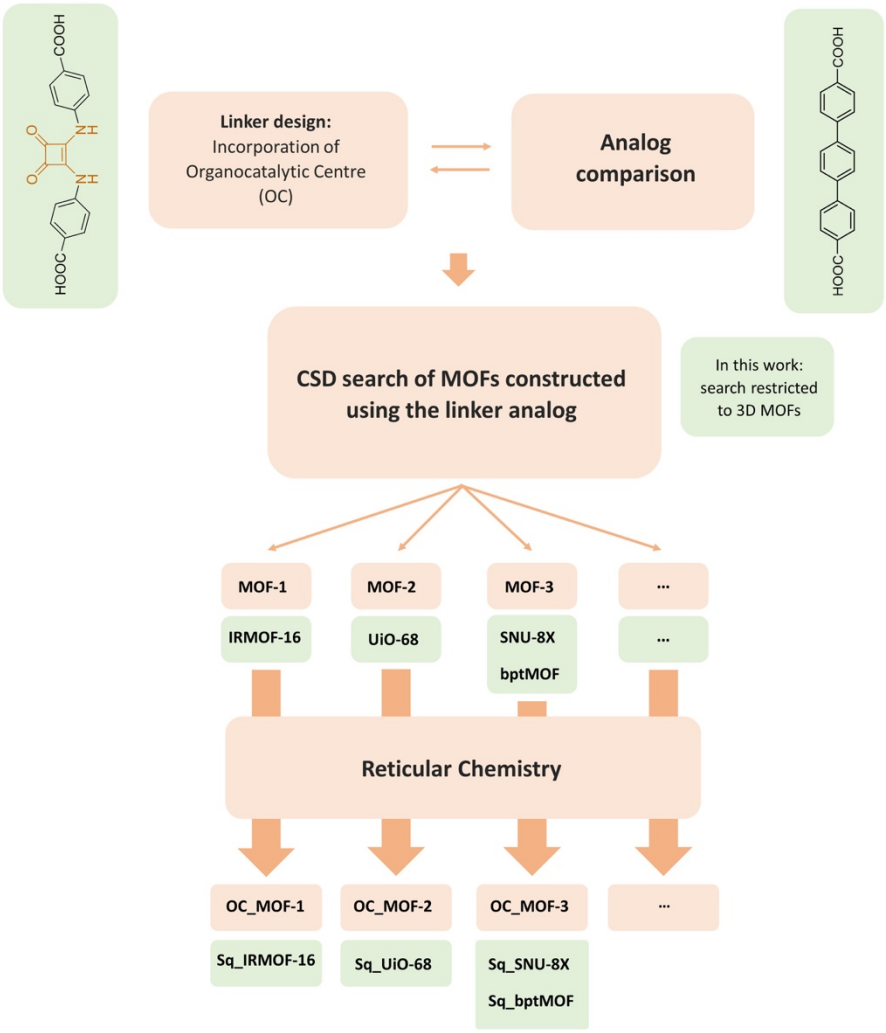

Figure 1. The reticular chemistry-based strategy for rational design of MOF-based catalysts containing organocatalytic centers. CSD: Cambridge Structural Database.

Broto et al., Figure 2

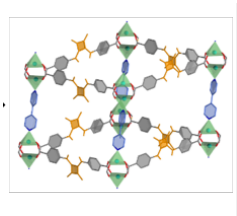

Figure 2. Representation of the crystal structures and cavities/pores of the MOFs and their corresponding isoreticular analogs (containing the squaramide rings): **IRMOF-16** and **Sq_IRMOF-16** (a); **UiO-68** and **Sq_UiO-68** (b); **SNU-8X** and **Sq_SNU-8X** (c); and **OZASUF** and **Sq-bptMOF** (d).

Broto et al., Figure 3

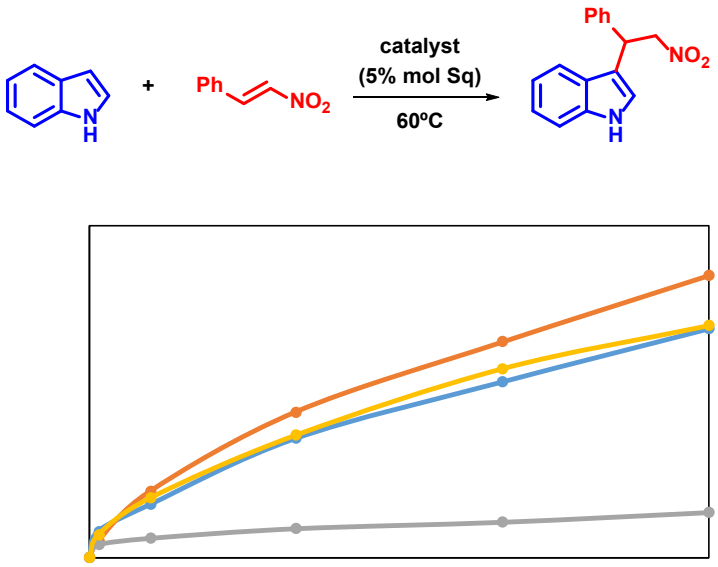

Figure 3. Kinetic plots for the Friedel-Crafts reaction of indole and β-nitrostyrene at 60 ºC, forming the alkylated product, in the presence of **Sq_IRMOF-16** (yellow), **Sq_SNU-8X** (orange), **Sq_UiO-68** (blue) or **Sq_bptMOF** (grey).

Broto et al., Figure 4

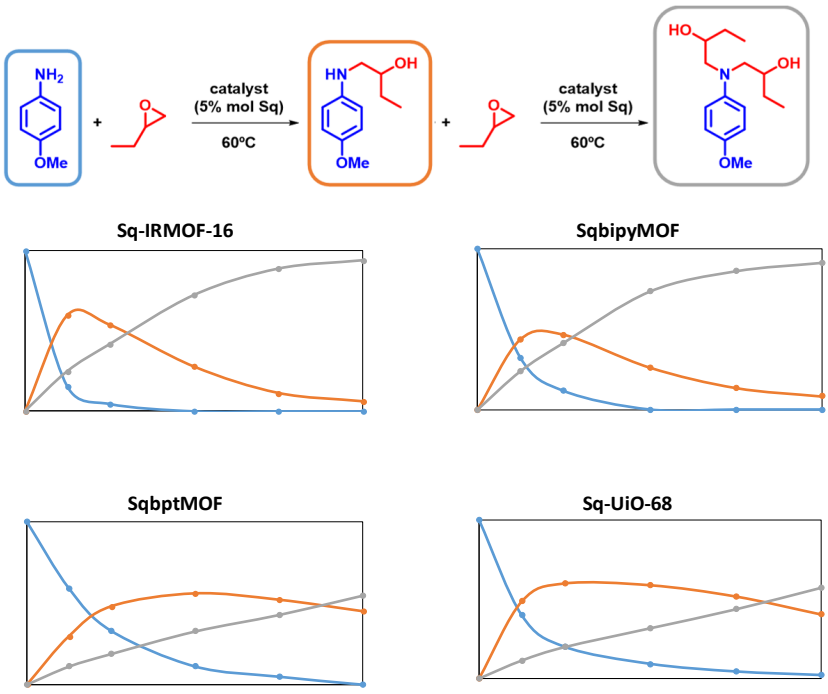

Figure 4. Kinetic plots for the epoxide ring-opening reaction of 4-methoxy aniline (blue) and ethyl epoxide at 60 °C to form the mono-adduct (orange) or bis-adduct (grey) product, in the presence of **Sq_IRMOF-16**, **Sq_SNU-8X**, **Sq_UiO-68** or **Sq_bptMOF**.